Schmandt et al., http://www.jgp.org/cgi/content/full/jgp.201511478/DC1

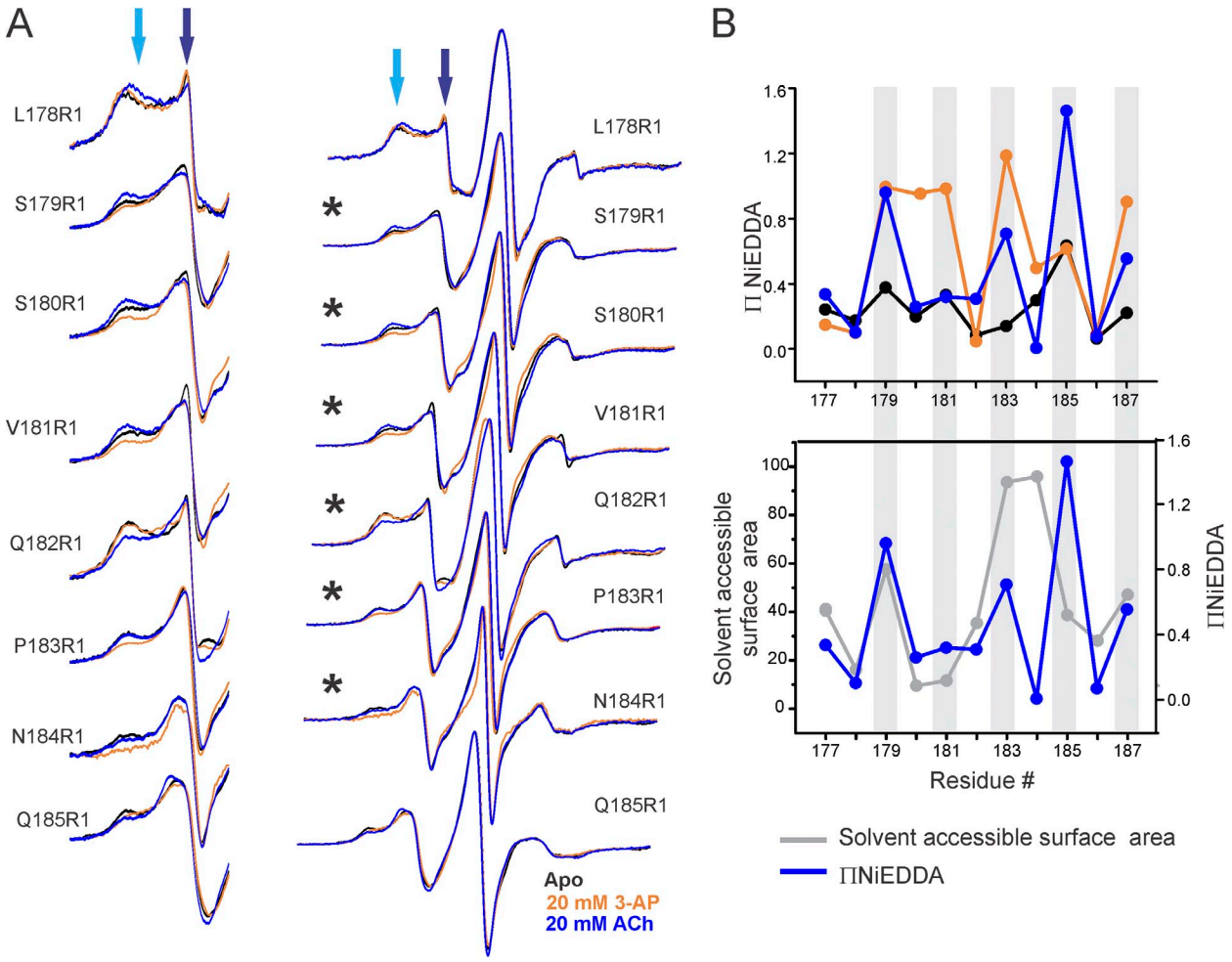

Figure S1. Changes in loop C dynamics and accessibility upon binding agonist and competitive antagonist. (A) An overlay of amplitude-normalized CW-EPR spectra of ELIC loop C mutants in the apo form and in the presence of either 20 mM 3-AP or 20 mM ACh. On the left is a zoomed-in view of the low field region. Light and dark blue arrows indicate the immobile and mobile components, respectively. Asterisks highlight positions revealing most prominent changes. (B) NiEDDA accessibility in the three conformations (top). A comparison of NiEDDA accessibility in the ACh-bound form with the calculated solvent-accessible surface area of loop C residues in the ACh-bound ELIC (PDB accession no. 3RQW). Solvent-accessible surface area calculations were done using the GETAREA program (Fraczkiewicz and Braun, 1998).

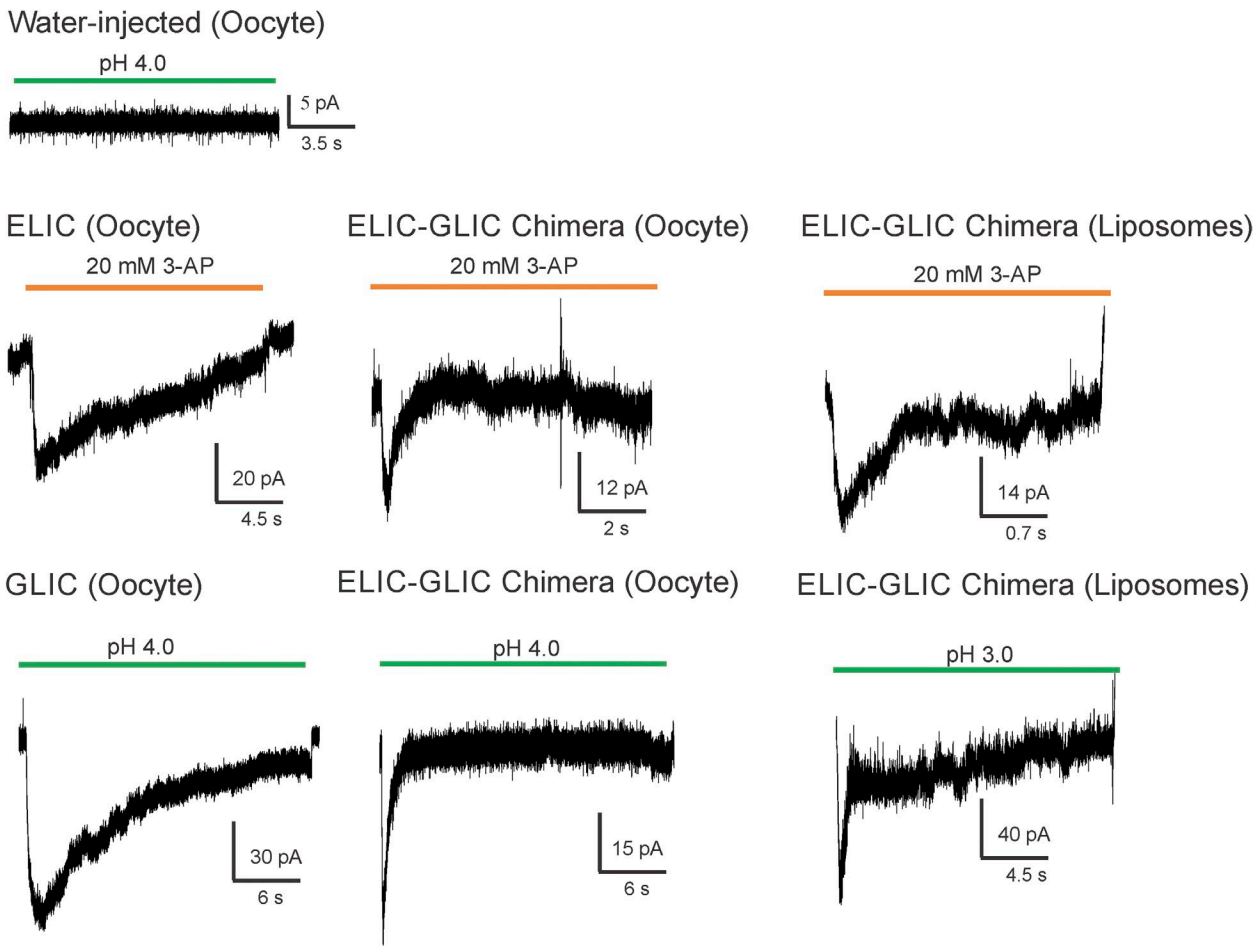

Figure S2. Patch-clamp measurements of ELIC, GLIC, and the ELIC-GLIC chimera. Macroscopic currents were measured from excised oocyte patches using a rapid solution exchanger to deliver the ligands (protons/3-AP). Time constants for current decays in ELIC and GLIC are 14.35 ± 2.37 s (n = 3) and 9.84 ± 4.20 s (n = 6), respectively. The decay time constant for the chimera activated by protons is 0.83 ± 0.29 s (n = 3) and by 3-AP is 0.64 ± 0.3 s (n = 3). Inset shows currents recorded from excised patches of reconstituted proteoliposomes using previously described methods (Velisetty and Chakrapani, 2012; Velisetty et al., 2012, 2014).

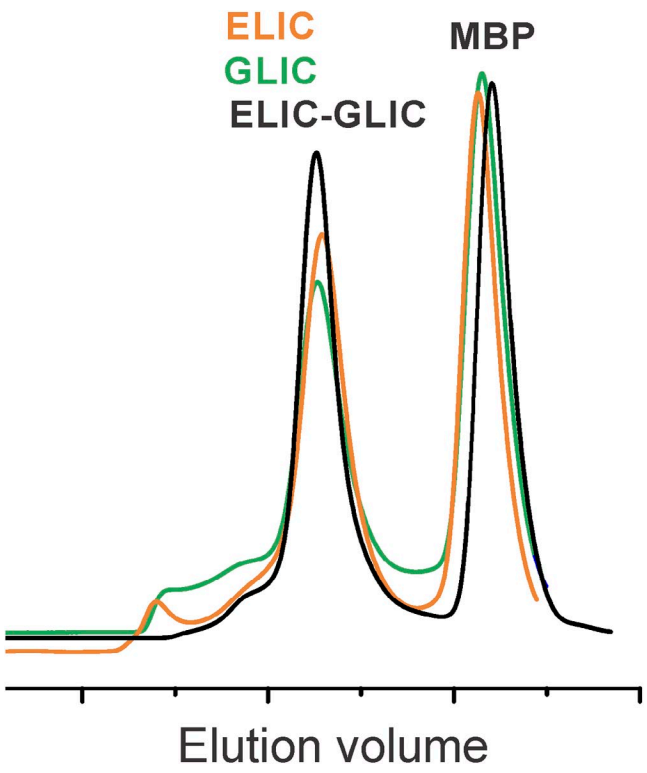

Figure S3. Biochemical characterization of the ELIC-GLIC chimera. Gel-filtration chromatograms of ELIC, GLIC, and ELIC-GLIC after proteolytic cleavage of maltose-binding protein (MBP) tag. The channel peak corresponds to the pentameric population.

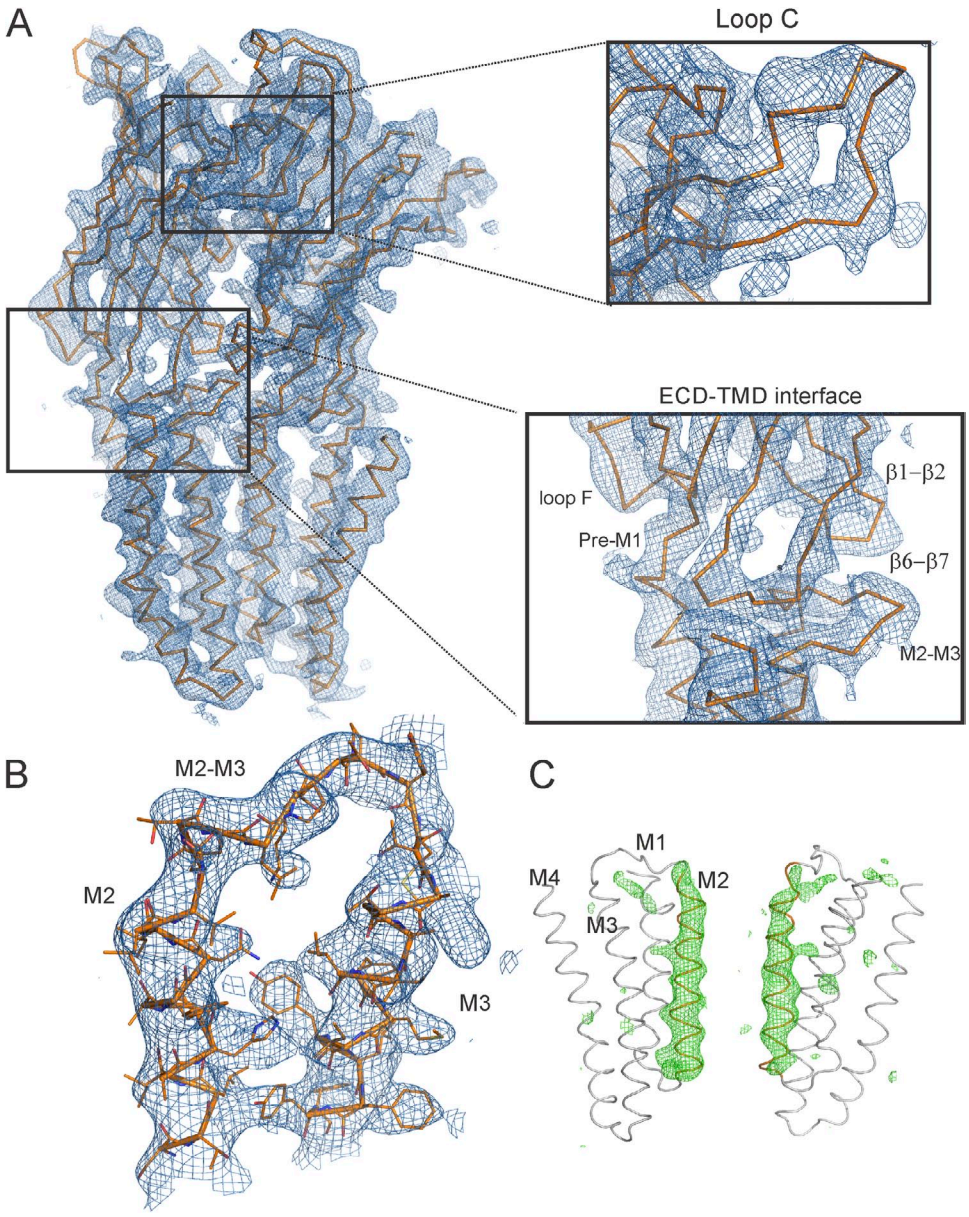

Figure S4. Electron density in key regions of the ELIC-GLIC chimera. (A) The ELIC-GLIC chimera is shown in ribbon representation (only two subunits displayed for clarity). The blue mesh is the maximum likelihood 2m|Fo|-D|Fc| electron density map contoured at a level of 1.0 σ (left). Magnified views of loop C and the ECD–TMD interface and the 2m|Fo|-D|Fc| map contoured at 1.0 σ (right). (B) Magnified view of M2, M2–M3 linker, and M3, and the 2m|Fo|-D|Fc| map contoured at 1.0 σ. (C) The side view of the TMD. The green mesh is the m|Fo|-D|Fc| density map calculated with the M2 region omitted from the model and contoured at 3.0 σ.

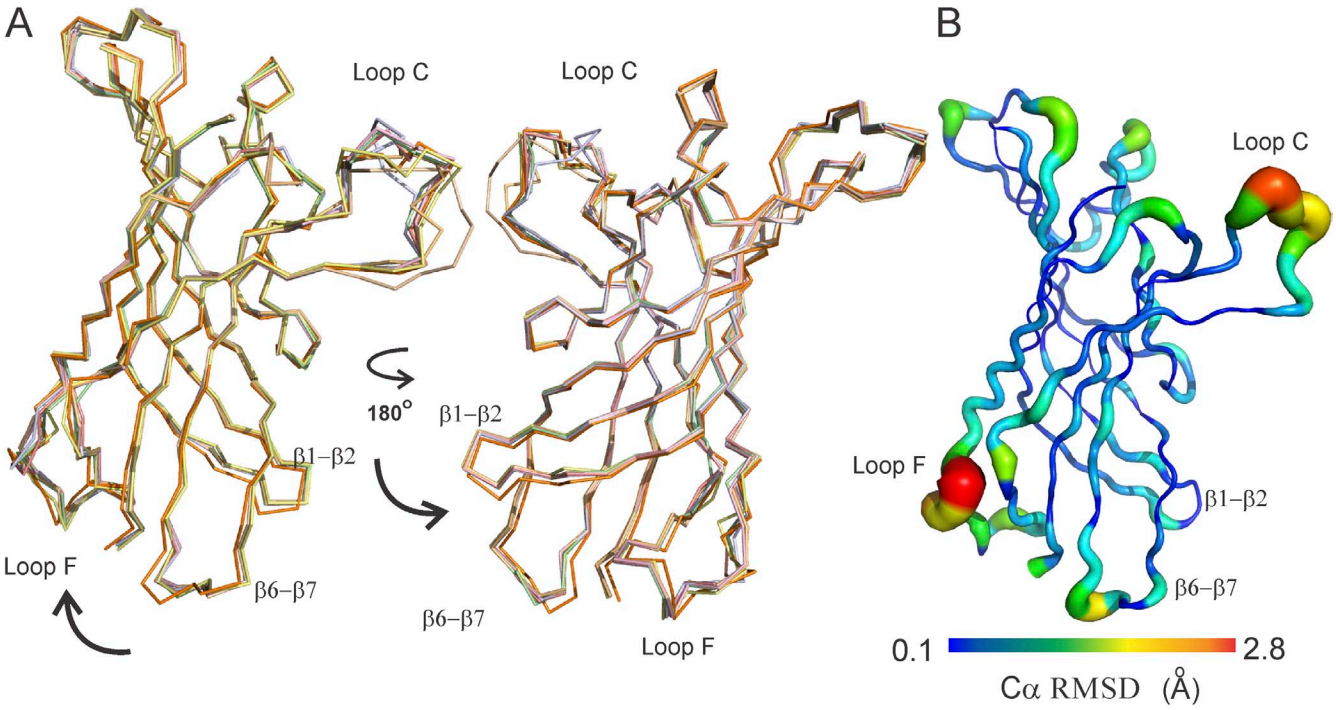

Figure S5. Quaternary twist in the ELIC-GLIC chimera ECD. (A) A superimposition of ECD chain A from the apo- and ligand-bound ELIC structures (PDB accession nos.: pale green, 2VL0; salmon red, 3RQU; light blue, 3RQW; light orange, 4A97; wheat, 4A98; pale yellow, 2YN6; pink, 2YOE), with the ECD of the ELIC-GLIC chimera shown in orange. The arrows indicate the direction of twist. (B) The Cα RMSD (chain A–ECD) deviation between apo-ELIC (PDB accession no. 2YN6) and the ELIC-GLIC chimera calculated using the Superpose program within CCP4 Suite (Krissinel and Henrick, 2004) and mapped on the chain A of the chimera crystal structure.

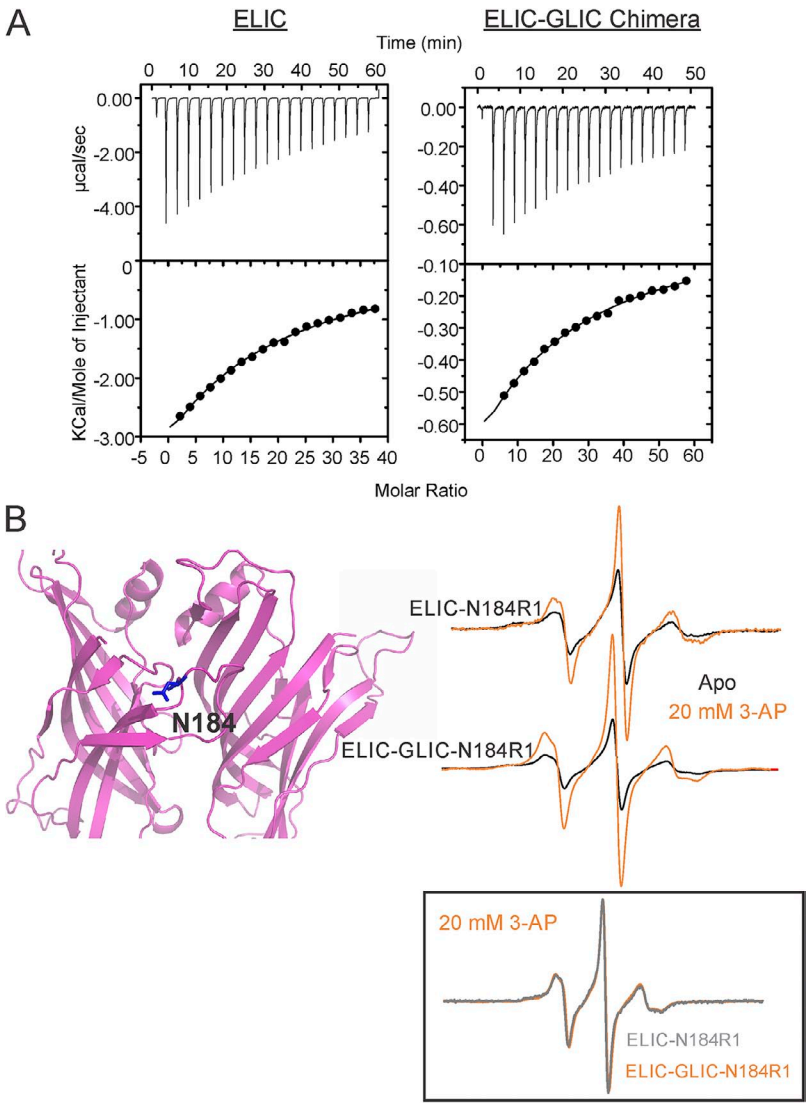

Figure S6. Agonist sensitivity of the ELIC-GLIC chimera is similar to ELIC. (A) Equilibrium-binding isotherms for ELIC and the ELIC-GLIC chimera titrated against 3-AP. The solid curves represent fits to a single-site binding isotherm with K_D of 2.16 ± 0.05 mM (ELIC) and 3.13 ± 0.03 mM (ELIC-GLIC chimera). (B) Agonist elicits similar structural changes at loop C in ELIC and ELIC-GLIC (right). Location of Asn184 is shown in the ELIC structure (left). Inset shows an overlay of amplitude-normalized N184R1 spectra at 20 mM 3-AP in ELIC and in the ELIC-GLIC chimera.

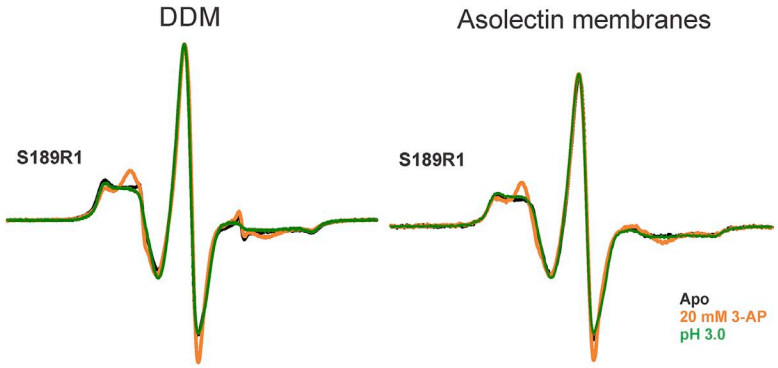

Figure S7. Spectral changes at Ser189 measured in detergent and liposome. Amplitude-normalized CW spectra for position Ser189 measured under the indicated conditions for the sample in DDM and in reconstituted asolectin membrane.

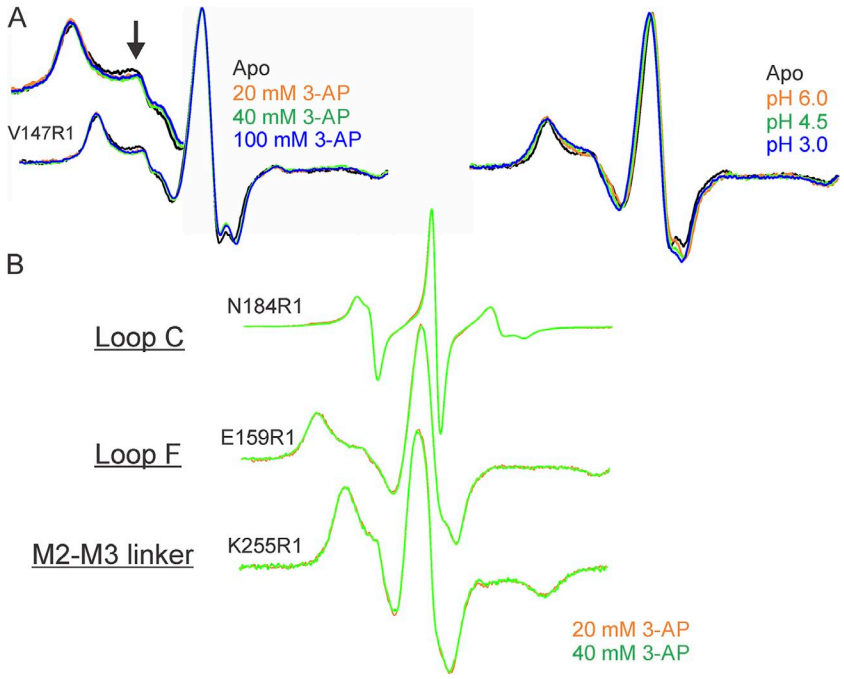

Figure S8. Ligand-induced spectral changes in the ELIC-GLIC chimera. (A) Amplitude-normalized spectra at V147R1 recorded at the indicated concentrations of 3-AP. Line-shape changes saturate at 20 mM 3-AP. No further changes are observed at 40 and 100 mM 3-AP (left). Amplitude-normalized V147R1 spectra at various pH conditions. pH-induced changes are identical between pH 4.5 and 3 (right). (B) Amplitude-normalized spectra at representative positions in the ELIC-GLIC chimera in the presence of 20 or 40 mM 3-AP.

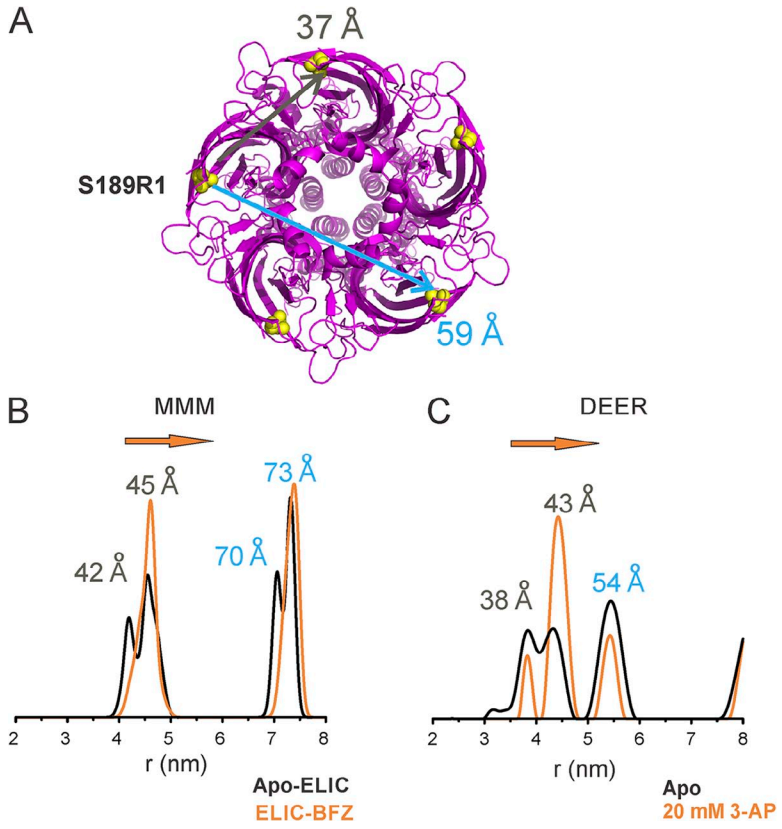

Figure S9. Rotamer simulation for Ser189 using MMM. (A) Cartoon shows the position of S189 in the apo-ELIC structure (PDB accession no. 3RQU) and the Cβ-Cβ–adjacent and –diagonal distances. (B) Simulation of interspin distance distribution using the MMM package for labels at position Ser189 in the apo ELIC structure (PDB accession no. 3RQU) and in the benzodiazepine-bound ELIC (PDB accession no. 4A98). (C) Distance distribution measured by DEER in the apo- and 3-AP–bound forms.

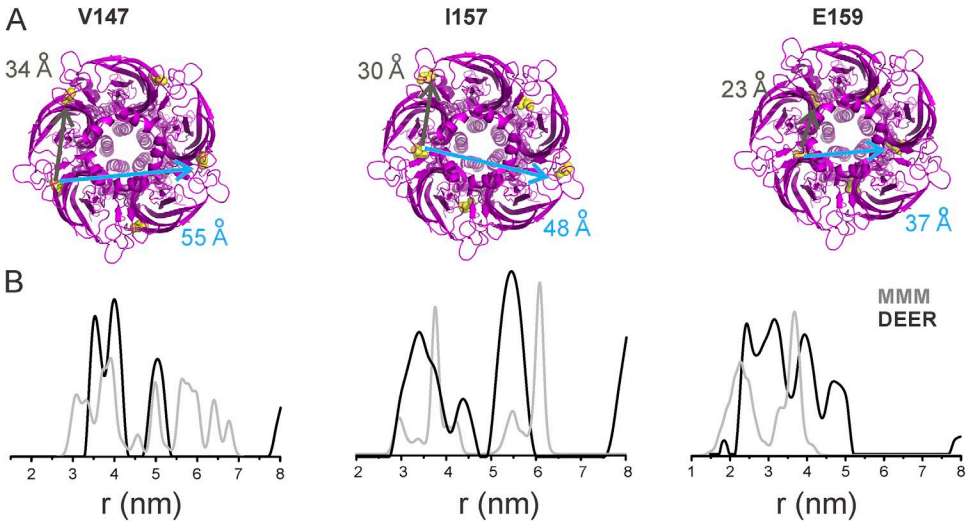

Figure S10. Rotamer simulation for loop F mutations. (A) Cartoon shows these positions in the apo-ELIC structure (PDB accession no. 3RQU) and the Cβ-Cβ–adjacent and –diagonal distances. (B) MMM simulation of distance distribution for spin label at positions Val147, Ile157, and Glu159 in the apo-ELIC structure (PDB accession no. 3RQU) is shown in gray. Distance distribution measured by DEER in the apo form is shown in black.

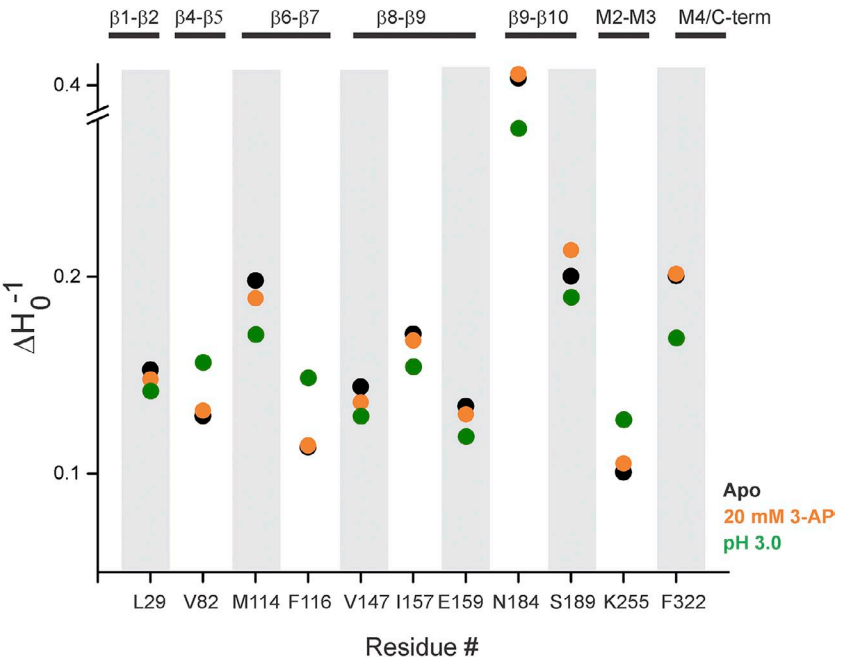

Figure S11. Mobility changes in the Apo, 3-AP, and pH 3.0 conditions. A plot of the inverse of the central line width in the CW-EPR spectra at various positions in the ELIC-GLIC chimera measured in the apo and liganded conditions.

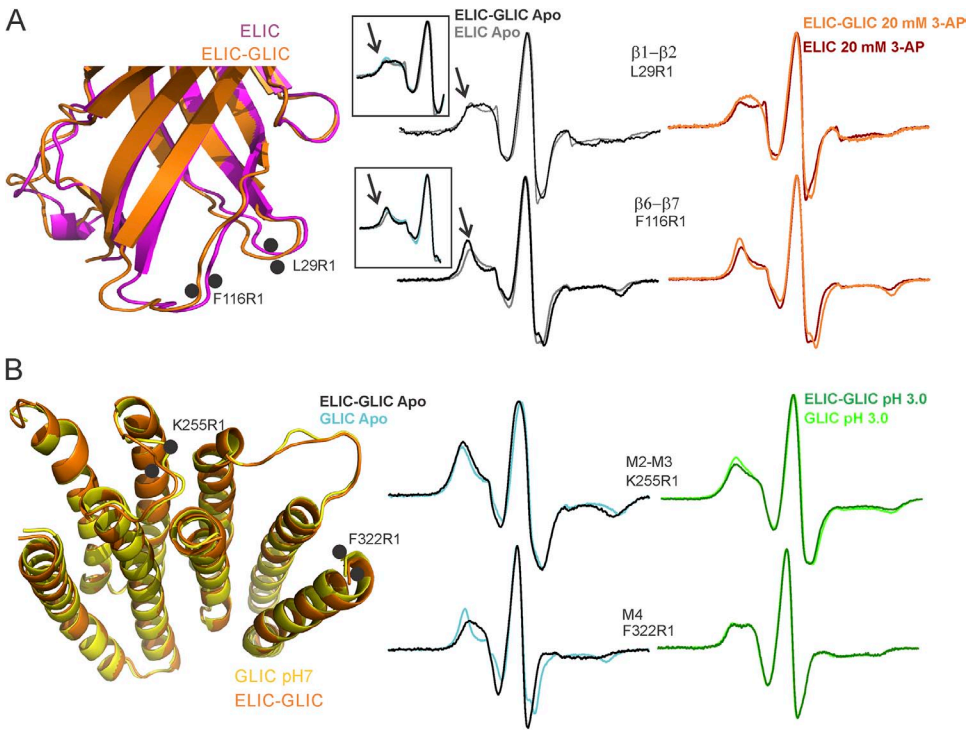

Figure S12. Changes in the ECD–TMD interface dynamics in the ELIC-GLIC chimera compared with ELIC and GLIC. (A) Superposition of apo-ELIC (PDB accession no. 2YN6) and the ELIC-GLIC chimera (left). An overlay of amplitude-normalized EPR spectra for the chimera and ELIC in the apo and 3-AP conditions. Inset shows a zoomed-in view of the low field component. Light blue trace is the spectra from GLIC at the corresponding positions. Arrow points at the immobile component. (B) Superposition of GLIC–pH 7.0 (PDB accession no. 4NPQ) and the ELIC-GLIC chimera (left). Amplitude-normalized EPR spectra for the chimera and GLIC in the apo and pH 3.0 conditions.

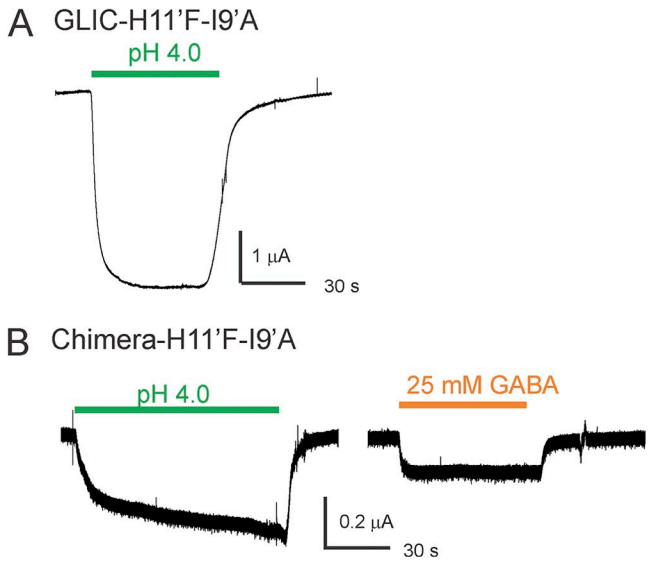

Figure S13. I9'A rescues the function of H11'F mutation both in GLIC and in the ELIC-GLIC chimera. (A) Oocyte current recording for GLIC H11′F/I9′A double mutant. (B) pH and GABA response for the ELIC-GLIC chimera in the presence of H11′F/I9′A background mutations.

TABLE S1

Data refinement and statistics

	ELIC-GLIC (PDB accession no. 4YEU)
Data collection	
Beamline	NE-CAT 24-ID-C/E
Wavelength	0.97918
Space group	$C222_1$
Cell dimensions *a*, *b*, *c* (Å)	132.4, 218.0, 229.6
No. of observations[a]	433,934
No. of unique observations	18,904
Resolution range (Å)	49.22–4.59 (5.03–4.59)
$CC_{1/2} = 0.5$ (Å)[b,c]	4.59
$CC_{1/2} = 0.5$ on h axis (Å)[d]	4.81
$CC_{1/2} = 0.5$ on k axis (Å)[e]	5.19
$CC_{1/2} = 0.5$ on l axis (Å)[f]	4.59
Mean I/σ (I)	9.7 (1.3)
R_{pim}[g]	0.041 (0.754)
Completeness (%)	99.9 (99.8)
Multiplicity	23.0 (13.6)
Average mosaicity	0.19
Refinement[h]	
Resolution (Å)	20.0–4.60
R_{work} (%)	24.17
R_{free}[i] (%)	24.85
Number of atoms	12,825
RMS deviations:	
Bond lengths (Å)	0.008
Bond angles (°)	0.98
MolProbity score[j]	99th percentile
Ramachandran analysis[k]	
Favored	87.0%
Allowed	12.0%
Generously allowed[h]	1.0% (14 residues)

[a]Number of observations is the sum of observations from the component datasets. Because of extreme anisotropy, six data sets were scaled together.

[b]$CC_{1/2}$ is the Pearson correlation coefficient of two-half data sets (Karplus and Diederichs, 2012).

[c]I/σ $(I) = 2$, 4.99 overall.

[d]$I/\sigma(I) = 2$, 4.91 on h axis.

[e]$I/\sigma(I) = 2$, 5.38 on k axis.

[f]$I/\sigma(I) = 2$, 4.96 on l axis.

[g]R_{pim} (within I+/I−).

[h]Two TLS groups (consisting of residues 11–199 and 200–322) per monomer were used, and between rounds of refinement, the B factors were set to 150 $(Å)^2$ for the residues in the ECD and 100 $(Å)^2$ for the residues in the TMD.

[i]5.13% of reflections was excluded from refinement for calculation of R_{free}.

[j]Molprobity Score (Chen et al., 2010) for structures in the resolution range of 3.25–4.85 Å.

[k]Calculated using PROCHECK (Laskowski et al., 1993).

REFERENCES

Chen, V.B., W.B. Arendall III, J.J. Headd, D.A. Keedy, R.M. Immormino, G.J. Kapral, L.W. Murray, J.S. Richardson, and D.C. Richardson. 2010. MolProbity: all-atom structure validation for macromolecular crystallography. *Acta Crystallogr. D Biol. Crystallogr.* 66:12–21.

Fraczkiewicz, R., and W. Braun. 1998. Exact and efficient analytical calculation of the accessible surface areas and their gradients for macromolecules. *J. Comput. Chem.* 19:319–333. http://dx.doi.org/10.1002/(SICI)1096-987X(199802)19:3<319::AID-JCC6>3.0.CO;2-W

Karplus, P.A., and K. Diederichs. 2012. Linking crystallographic model and data quality. *Science.* 336:1030–1033. http://dx.doi.org/10.1126/science.1218231

Krissinel, E., and K. Henrick. 2004. Secondary-structure matching (SSM), a new tool for fast protein structure alignment in three dimensions. *Acta Crystallogr. D Biol. Crystallogr.* 60:2256–2268. http://dx.doi.org/10.1107/S0907444904026460

Laskowski, R.A., M.W. Macarthur, D.S. Moss, and J.M. Thornton. 1993. Procheck: a program to check the stereochemical quality of protein structures. *J. Appl. Cryst.* 26:283–291. http://dx.doi.org/10.1107/S0021889892009944

Velisetty, P., and S. Chakrapani. 2012. Desensitization mechanism in prokaryotic ligand-gated ion channel. *J. Biol. Chem.* 287:18467–18477. http://dx.doi.org/10.1074/jbc.M112.348045

Velisetty, P., S.V. Chalamalasetti, and S. Chakrapani. 2012. Conformational transitions underlying pore opening and desensitization in membrane-embedded *Gloeobacter violaceus* ligand-gated ion channel (GLIC). *J. Biol. Chem.* 287:36864–36872. http://dx.doi.org/10.1074/jbc.M112.401067

Velisetty, P., S.V. Chalamalasetti, and S. Chakrapani. 2014. Structural basis for allosteric coupling at the membrane-protein interface in *Gloeobacter violaceus* ligand-gated ion channel (GLIC). *J. Biol. Chem.* 289:3013–3025. http://dx.doi.org/10.1074/jbc.M113.523050